Interleaved Continuum-Rigid Manipulation: An Approach to Increase the Capability of Minimally Invasive Surgical Systems

Benjamin L. Conrad, *Student Member, IEEE*, and Michael R. Zinn, *Member, IEEE*

***Abstract*—Continuum manipulator compliance enables operation in delicate environments while challenging the actuation and control approaches. In the case of a catheter ablation of atrial fibrillation, the compliance of the continuum backbone lends an inherent safety to the device. This inherent safety frustrates attempts at precise, accurate, and fast control, limiting the continuum devices to simple and static positioning tasks. This paper develops interleaved continuum-rigid manipulation, by which the hysteretic nonlinearities encountered in tendon-actuated continuum manipulators are compensated by the discrete rigid joints located between the continuum sections. The rigid joints introduce an actuation redundancy, which an interleaved controller may use to avoid the continuum nonlinearities and dynamic excitations, or to prefer particular configurations that may improve task accuracy, permit greater end-effector forces, or avoid environment obstacles. Two experimental systems explore the potential of these joints to: 1) increase the manipulator's dexterous workspace, and 2) correct for actuation nonlinearities and enhance manipulator performance. These experiments also expose important design and control observations that were not apparent in the general robotic and continuum literature.**

***Index Terms*—Actuators, control engineering, dexterous manipulators, medical robotics, redundant systems.**

I. Introduction

ROBOTIC cardiac catheter systems operate within a patient's beating heart, accessing tissue with substantially less invasivity than open-heart procedures. In this and other applications, manipulator compliance is essential, and all remaining design freedoms are spent improving accuracy, response speed, and force capability. This paper introduces interleaved continuum-rigid manipulation as a concept to enhance the capabilities and performance of the continuum manipulator systems without compromising their essential compliance.

Manuscript received February 22, 2016; revised May 19, 2016; accepted August 6, 2016. Date of publication September 12, 2016; date of current version February 14, 2017. Recommended by Techinical Editor D. Stoianovici. This work was supported by the National Science Foundation under Grant IIS-1316271.

The authors are with the Department of Mechanical Engineering at the University of Wisconsin, Madison, WI 53706 USA (e-mail: bconrad@wisc.edu; mzinn@wisc.edu).

Color versions of one or more of the figures in this paper are available online at http://ieeexplore.ieee.org.

Digital Object Identifier 10.1109/TMECH.2016.2608742

The motive application for this work is the treatment of atrial fibrillation (AF) via cardiac catheter systems, but as we are concerned with increasing the capability of the tool the conclusions can be applied to other minimally invasive operations in the heart and continuum manipulation more broadly (see [1] for a recent overview). AF is characterized by the rapid erratic beating of the heart due to errant heart muscle signaling and muscle activation (see [2]–[4] for longer discussions of the intervention and efficacy). The discordant beating results in decreased pumping efficiency, greater organ, and system stress, and reduced quality of life [2]. Treatment typically involves ablating tissue around each of the pulmonary vein ostia by a physical contact with an ablation probe; the resulting lesion is less conductive than normal tissue and thereby blocks the errant signaling. Successful treatment requires contiguous and transmural (spanning the heart wall thickness) lesions and is therefore a function of the device performance and controllability.

AF interventions are performed most commonly by tendon-actuated catheters. The primary structure is an elastic backbone that is long with respect to its diameter, having low bending stiffness while resisting axial compression and torsion. The low bending stiffness gives the manipulator an *inherent safety*, accepting unknown anatomical contacts without tissue damage. A central lumen provides a toolpath, with the actuation tendons routed along the periphery through the actuation lumens. With the tendons terminated at the distal end, applying tensions to the tendons induce bending. The long sliding interface between the tendon and guiding lumen leads to highly nonlinear and nonstationary hysteresis that varies with the configuration and ultimately limits catheter performance and disturbance rejection.

Despite the efficacy of catheter-based interventions and the commercial success of several companies, fundamental challenges limit the performance and prevent their wider use. We seek improved accuracy, precision, and response speed over today's tendon-actuated manipulators that permit disturbance rejection at appropriate time scales ($<$1 s) and enable teleoperation (closed-loop bandwidths $>$10 Hz). Prior efforts to improve tendon-actuated continuum manipulator performance have focused on improving open-loop performance via design, better kinematic, and dynamic modeling, and various forms of control, with each avenue benefiting from improvements in the others.

A. Design Yields Modest Performance Improvements

Numerous attempts have been made to avoid[1] or reduce hysteresis through design, especially commercially. Recognizing that friction loads increase with articulation, designers may decrease bending stiffness and suffer greater torsion and axial compliance, or refine the tendon/lumen sliding interface through material and lubricant selection. These design trades are unique to each product and are not discussed in the literature; also, commercial devices have not been benchmarked at the level of physical performance but rather at more nebulous levels of intervention efficacy. There are no widely accepted and utilized benchmarks for catheter performance; a variety of measures are borrowed from the evaluation of the traditional robotic manipulators (precision, accuracy, speed, bandwidth, disturbance rejection ratio, etc.), but their application often suffers from operating point effects. This is due to the present insufficient understanding of the acting phenomena (described next) and the one-off or proprietary nature of systems described in the literature; this limits communication and design, model, and controller comparison. One anecdote is the good static performance of [6], [7] achieved with a catheter from Hansen Medical, Inc., though no dynamic tracking results are presented. Beyond this, designing the tendon/lumen sliding interface is challenged by space constraints and the necessity of biocompatible and sterilizable materials. It appears, then, that conscientious design can *incrementally* improve tendon-actuated catheter performance, but has not yet grasped the desired order-of-magnitude improvements.

B. Accurate Modeling is Difficult

The literature has attempted to model the interaction between the elastic backbone and articulating tendon, see [8] for a review. Camarillo *et al.* [6] were the first to closely consider tendon actuation of a continuum manipulator and achieved good experimental agreement; the resulting mechanics model, however, ignores friction and therefore performs best at low articulations. In a recent effort, Subramani and Zinn [9] explicitly modeled Coulomb friction between the tendon and guide lumen. Jung *et al.* [10] developed a dynamic lumped-parameter model to explore friction in a four tendon catheter whose articulating length could be changed by extension from a rigid proximal sheath. The numerical approach allowed the use of a Dahl friction model and consideration of tendon stretch along the catheter length, resulting in a very good prediction of static and dynamic catheter configurations—after lengthy computations. Dynamic motion across the manipulator workspace exceeds these efforts, particularly at high articulations ($>90^\circ$) where the greatest frictional forces occur. The modeling challenge justifies spending substantial effort reducing or designing-out these nonlinearities.

C. Advanced Control May Double Performance

The modest improvements achieved through the improved modeling and design suggest similarly limited increases from advanced control architectures. Closest to application are efforts that model system nonlinearities generally, considering only a resulting behavior (like a hysteresis loop) rather than the originating phenomena. Khoshnam and Patel [11] develops a system that manipulates a commercial manual catheter and compensates for the patient's heartbeat by estimating the catheter articulation delay and articulation error (both resulting from catheter and tendon compliance). Kesner and Howe [12] developed a 1-D feedforward guidewire position controller that compensates for heart motion. The modeled sliding friction and backlash were then used in a feedforward controller to compensate the desired command against these losses.

Related are efforts that attempt to learn the forward and/or inverse kinematics (IK); Melingui *et al.* [13] and Rolf and Steil [14] demonstrate impressive results controlling Festo's pneumatic Bionic Handling Assistant. Closer to our interest is Giorelli *et al.*'s [15] application of a neural network to learn the static relationship between tendon force and tip position in a tapered and tentacle-like tendon-actuated manipulator segment. Bian *et al.* [16] used a feedforward neural network to learn the IK of an ablation catheter, though the lengthy training process exhausted the catheter's design life; the subsequent device failure indicates the challenge of learning on minimal training sets. The various learning techniques are fundamentally limited in their ability to consider actuation history: some take the instantaneous joint velocity as a model input, but this is incapable of describing nonstationary phenomena like hysteresis. Forms of repetitive or iterative learning control [17] have not yet been applied to the control of continuum manipulators; some less-periodic variants may be able to learn the temporal nonlinearities and improve the performance across the workspace, though assembling a sufficiently large training set may exceed device life (as observed in [11]).

Using one of the previously described modeling approaches enables control development within the model's limitations. This typically involves using a reduced-order model to design controllers that are conservatively tuned so as to remain within the simplified model and away from the unmodeled, unobserved, and unactuated degrees of freedom (DOF). For instance, assuming a constant curvature in a multisegment continuum manipulator allows Ivanescu *et al.* [18] to develop a sliding mode controller and show Nyquist stability, but dynamic performance and comparison to their numerical simulations are omitted. Falkenhahn *et al.* [19] provides a great example of the performance that may be attained when the physical phenomena are well understood, as they are in Festo's pneumatic Bionic Handling Assistant. In our case, the described limited mechanistic understanding of tendon-actuated catheters prevents linearization (or really any useful modification) of the catheter plant. Therefore, catheter controllers do not attempt to change the plant dynamics but are rather tuned to ensure task performance and disturbance rejection.

The preceding methods attempted to improve the forward open-loop path by better modeling or learning the manipulator's characteristics offline; these are complemented by efforts utilizing feedback in a closed-loop controller. In light of the hysteresis, tendon displacements measured proximal to the catheter are insufficient in determining the resultant manipulator configuration, and task position in particular. A task sensor is required;

[1]Longer term, it seems likely that some form of distributed actuation (as widely seen in biologic systems [5]) will supplant tendon-actuated catheters.

incorporating it into a real time, closed-loop controller leads to a noncollocated system where the position- or force-controlled drives are separated from the sensor by the backbone compliance, hysteresis, and other nonlinearities [20], [21]. Considering only the continuum backbone, intuition quickly shows that the vibrational modes shift with articulation and that the lowest changes from planar bending to torsional—from an actuated to an unactuated DOF—as continuum manipulators do not actively control the backbone twist [22].

The challenge of measuring the external disturbances and internal tendon loads results in a structure with poorly known loadings and an essentially unpredictable dynamic behavior. Without excellent knowledge of the configuration, loading, and various nonlinearities, it is practically impossible to operate the system above the lowest vibrational mode. To this, Preumont [22] developed a modal controller that used measurements of the first and second bending modes to dampen the first mode. The architecture allowed operation above the first vibrational mode, increasing the closed-loop bandwidth from 1.1 to 2.6 Hz for, again, an incremental performance improvement. The increased computational and sensing burden leads most tendon-actuated continuum controllers to operate beneath the first mode in the manipulator's quasi-static linear domain. Some form of integral control enables task tracking and the elimination of dc error, while damping from the tendon/lumen friction is often sufficient to ensure the stability. Other controllers may be posed, but no real improvements are possible without improved dynamic modeling and/or prediction inclusive of the actuating mechanism.

Careful design and fabrication, physically motivated modeling, and advanced control all have resulted in only incremental improvements in response speed and accuracy. These good efforts suggest that the available design freedoms are too constraining.

II. Interleaved Continuum-Rigid Manipulation

Reflection on the many challenges of tendon-actuated continuum manipulators motivated a reevaluation of the fundamental manipulator design. Recognizing the limitations of continuum manipulators in the literature, while still desiring to perform more advanced tasks, we advocate interleaved continuum-rigid manipulation which complements the inherent safety and large workspace of the flexible catheter segments with the precision and speed of the traditional revolute and prismatic joints (see [23] for general observations on the utility of continuum and discrete joints). In the interleaved manipulator of Fig. 1, the flexible continuum segments access a large workspace while compliantly—and safely—interacting with tissue. The redundantly arranged rigid joints are easily modeled and easily controlled, permitting compensation of flexible segment nonlinearities.

This concept introduces a new design and actuation freedoms, resulting in a variety of improved capabilities. Substantially increased dexterous workspace is immediately apparent; as mentioned in [24], even minimal rigid joint ranges of motion greatly expand the dexterous workspace over continuum-only manipulators with the same DOF. Dexterity is useful: end-effector-posed regulation is quite impractical

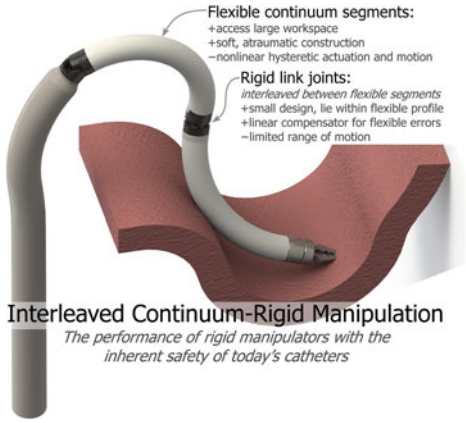

Fig. 1. Notional interleaved continuum-rigid manipulator addressing tissue.

with continuum-only manipulators but reasonable under an interleaved approach. This concept newly enables the introduction of redundancy to facilitate obstacle avoidance and contact-choosing (so as to prefer contacting stationary or thicker tissue). Increased task performance (improved response speed, accuracy, and precision) is also evident—as the continuum sections can be as performant as those in continuum-only manipulators—though realizing increased performance challenges control design (as Section IV details).

Viewed through a more fundamental lens, this design approach represents an attempt to decouple the inherent safety of the underactuated continuum structure from the challenge of accurately actuating that same structure.

Interleaved manipulators inhabit the design space between safe, distributed actuation, flexible-link continua, and conventional rigid-link manipulators, varying link compliance and joint design by application. Populating this manipulator design spectrum—and determining ideal control architectures along it—will be the subject of the ongoing work.

While the stiffness of the continuum elements in any interleaved manipulator may be easily tuned, the critical burden is to design structures and joints so that they achieve the required stiffness and precision within the device profile. The challenge in designing compact rigid joint actuators appears to favor limited stroke, high output impedance approaches; piezoelectric actuators are an obvious candidate among many. In the near-term, we expect that the rigid joints will generally be of greater precision, have less actuation range, and be faster than the flexible segments. In the remainder of this paper, we explore interleaved continuum-rigid manipulation through two systems: the first, 5-DOF prototype showcases rigid joints integrated into the manipulator profile that increase the dexterous workspace, expose interesting control challenges, and conceptually ground the approach; the second, single-DOF testbed demonstrates possible performance gains when unrestricted by joint miniaturization.

III. Clinically Approximate Prototype Manipulator

This section actualizes the interleaved manipulation concept through the 5-D manipulator shown in Fig. 2. Numerous mechanism, actuator, transmission, and control concepts can be considered while designing an interleaved manipulator; this first

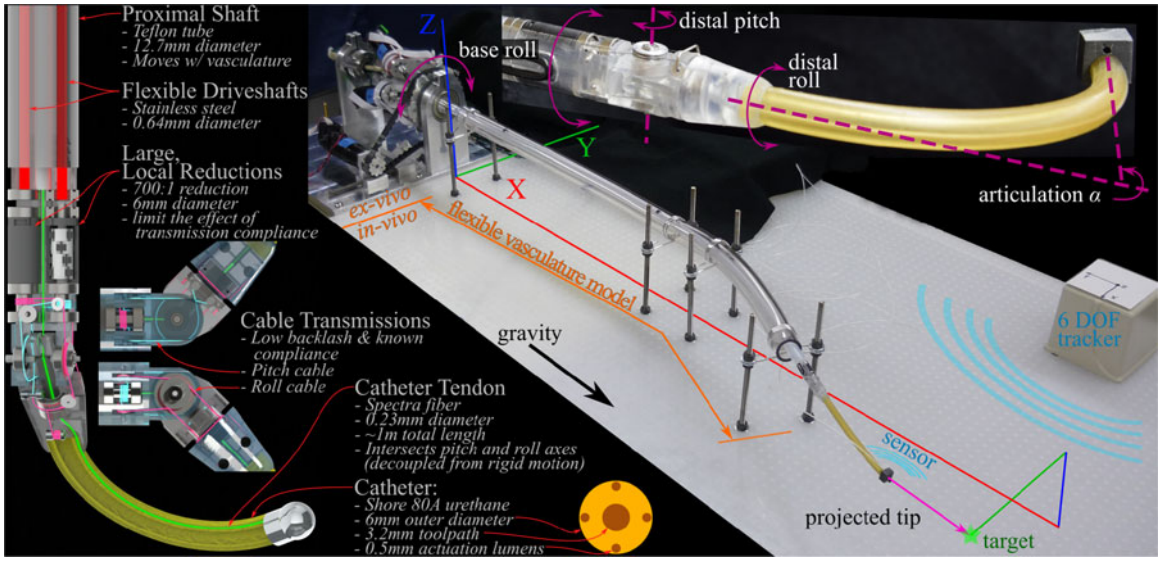

Fig. 2. Five-dimensional prototype interleaved continuum-rigid manipulator. The overall prototype is pictured at center, with the upper-right inset detailing the distal DOF, and the left section views illustrating the mechanical design. See text for further description.

attempt is conservative in each of these domains to accessibly show the concept's practicality.

The 5-DOF manipulator shown in Fig. 2 accesses a large workspace via two flexible segments (proximal shaft and catheter) with two rigid joints (distal pitch and roll) lying within the profile of the proximal elements. The fifth is a virtual prismatic joint formed by projecting along the catheter tip pointing vector. The prototype traverses a flexible vasculature model to the notional patient's heart, where the rigid joints and catheter operate. Four pin supports anchor and shape the vasculature model to generally mimic the path from the femoral vein to the right atrium. The pin supports and tube compliance move according to external (organ) forces and with rotations of the proximal shaft, capturing (to some degree) the variable transmission properties encountered in clinical devices. The *present* scarcity and immaturity of powerful actuators and encoders at $<$6 mm diameter scale motivates remote actuation of the rigid joints. Remote actuation locates the drives external to the patient, allowing unconstrained servo selection at the cost of longer transmission elements that accumulate errors that vary with vasculature configuration. In this prototype, large reductions in the rigid joints minimize these transmission errors by the reduction ratio, offering a trade between the rigid joint extent and performance (an increased gear reduction increases precision, accuracy, and extent while decreasing speed). In critical dimensions, the prototype of Fig. 2 is two to three times larger than the maximal clinical device because further minimization would have substantially increased cost, complicated fabrication, and assembly, and limited system inspection and performance evaluation.

We next describe the manipulator design in a greater detail, present a multiDOF controller, and show a target tracking experiment. Initial results of this prototype were shown in [25] and with improved rigid joints and a new controller in [24]. Building on these initial works, the following implements a general multiobjective IK solver in an integral task-space controller.

A. Touring the Manipulator Design

As above, the manipulator consists of two rigid joints and two flexible segments. The proximal roll joint is driven by a brushed 90-W dc gear motor (Maxon Motor AG, #273754) having a 18:1 reduction and a 500 count/turn encoder. This motor drives a timing belt with a further 3.2:1 pulley reduction, to which the proximal shaft connects. The proximal shaft is an 850-mm long 12.7-mm outer diameter Teflon tube with a 1.5-mm wall thickness, chosen for its torsional rigidity and bending stiffness. The distal pitch rigid joint is driven by a brushed 90-W dc motor (Maxon #273754) with 1024 counts/turn encoder connected to a 0.64 mm diameter by 890-mm long flexible stainless steel driveshaft. The distal end of this shaft drives a 699.5:1 planetary gearhead (Precision Microdrives #206-108) whose output connects to a cable transmission having a 2.6:1 reduction which drives the pitch joint. The distal roll rigid joint is identical to the distal pitch, with the exception of having a final cable reduction of 2.3:1. Both cables are made of 21 Tex bounded Kevlar thread (0.15 mm diameter, 25 N tensile strength, theThreadExchange.com). Fig. 2 details the rigid joint designs and shows how the catheter tendon intersects each of the proximal joint axes to decouple articulation from the joint actuation. The joints themselves consist of four three-dimensional (3-D)-printed parts detailed in Fig. 2 riding on miniature ball bearings and printed via a 3-D Systems Viper stereolithography system at 0.05 mm resolution. The pitch joint range of motion is $\pm 50^\circ$ and the distal rolls through $\pm 200^\circ$. (The ranges of motion, distal reduction, and rigid joint extent were chosen for convenience and not by an explicit trade.)

The 110 mm $\times$ 6.25 mm distal catheter is actuated by an 11-W dc gear motor (Maxon #222050) with a 109:1 planetary gearhead reduction and a 512 count/turn encoder. This gearhead turns a 12-mm diameter pulley to pull an approximately 1350-mm long tendon made of Teflon-coated 0.23-mm Honeywell Spectra woven fiber (sold as PowerPro braided

fishing line). Along the length of the proximal section, three thin-walled 3-mm Teflon tubes separate and loosely guide the two rigid joint driveshafts and the catheter tendon. The catheter is cast from Smooth-On PMC-780 urethane; Fig. 2 details the arrangement and sizes of the interior lumens. The Teflon-coated tendon exhibits substantially lower sliding friction against the urethane guiding lumen than that is typically found in the clinical catheters, partly due to the Teflon/urethane versus stainless steel/polyimide interfaces, but more substantially from the larger tendon/lumen clearance (0.23/0.50 mm) than is seen in clinical catheters (estimated as 0.25/0.31 mm from [26]). The first vibrational mode of this catheter is approximately 1.5 Hz measured at zero articulation and with all other joints undeflected and static. The motor position control loops are closed substantially above the system task bandwidth ($\sim$30 Hz $>$ 10 Hz) via a servo controller implemented in MATLAB xPC 2009 (The Mathworks, Inc.). Manipulator configuration is measured by an Ascension trakSTAR 6-DOF electromagnetic pose sensor mounted at the catheter tip operating at 300 Hz. The fifth virtual tip-to-target distance is projected along the tip pointing vector as measured by the pose sensor.

The large local reductions of the rigid joints are the defining aspect of this design; they determine the outer diameter (13 mm) of the rigid joints and permit accurate rigid joint actuation even under substantial proximal segment movement. The small diameter of the flexible driveshafts accept these movements at the cost of shaft windup prior to the reduction (approximately 50°/N·mm of shaft torque becoming 0.07°/N·mm after, according to linear elasticity). The shaft windup and large reduction introduce additional delay in the rigid joints; ignoring dynamic loads, this is tolerable as long as the resulting rigid joint bandwidths are a few times faster than the slowest flexible segment. Rigid joint cable compliance is more detrimental as it leads directly to the static and dynamic rigid joint errors; the Kevlar cables were tensioned to approximately 2 N such that no slack or joint play was noticeable. As seen in Fig. 2, the joints clearly lie within the profile of the proximal segment and the transition from the catheter is smooth, satisfying one of the basic rigid joint requirements.

B. Forward Kinematics (FK)

The manipulator is modeled by the homogeneous transformation matrices such that the tip position is given by ${}^0_5H = {}^0_1H\,{}^1_2H\,{}^2_3H\,{}^3_4H\,{}^4_5H$ with

$$
\begin{aligned}
{}^0_1H &= T_x(t_{x01})T_y(t_{y01})T_z(t_{z01})R_z(r_{z01})R_x(q_1)\\
{}^1_2H &= R_z(q_2)\\
{}^2_3H &= T_x(t_{x23})R_x(q_3)\\
{}^3_4H &= T_y\left(\frac{L_c}{q_4}\left(1-\cos q_4\right)\right)T_x\left(\frac{L_c}{q_4}\left(1-\sin q_4\right)\right)R_z(q_4)\\
{}^4_5H &= T_x(q_5)
\end{aligned}
$$

where $T*$ and $R*$ are homogeneous transformation matrices along or about the * axis, q_i is the ith joint position, and L_c is the length of the catheter. Referring to Fig. 2, ${}^0_1H$ transforms from the global XYZ to the axis of the distal pitch, about this axis ${}^1_2H$ rotates, after which ${}^2_3H$ translates to the roll joint and rotates about the roll axis, from which ${}^3_4H$ translates and rotates to the catheter tip, where ${}^4_5H$ finally projects to the target. Nominally, $t_{x01} = 811$, $t_{y01} = -157$, $t_z = -8.7$, $t_{x23} = 8.2$, $L_c = 110$ mm, and $r_{z01} = -21°$.

The simple geometric approach to the catheter FK assumes a constant catheter curvature and no tendon stretch.[2] This could be improved by using a mechanics-based model like those in [6] or [9] at an expense of the computation time. Appreciating this improvement would likely require modeling the entire manipulator with a similar rigor, an interesting task that is beyond our present aims.

C. Five Degree-of-Freedom Closed-Loop Controller

The overall controller topology is shown in Fig. 3; the task is to move the projected tip xyz to a position xyz^* in a 3-D space, as depicted in Fig. 2. The tip positions are formed from the filtered measured tip pose projected along the tip pointing vector the commanded tip-to-target distance (the virtual tip-to-target distance joint has no error). The resulting task-space error vector is integrated, gained, and added to the desired task. IK convergence to the task command produces a new set of joint angles which are executed by the manipulator. The outer loop is implemented in LabVIEW (National Instruments, Inc.) and runs at 10 Hz on a 3 GHz Intel Core 2 Duo. Joint angle commands q_{p*} are sent via UDP to the MATLAB xPC servo controller. The resulting pose is measured by the Ascension and communicated to the outer, LabVIEW loop over USB.

The task-space controller in Fig. 3 is so named because the outermost error and integral controller operate on the task vector, the projected tip *xyz* position. The use of an integral controller results from considering the system's first mode at approximately 1.5 Hz and desiring a crossover frequency as near to that as stability permits. More advanced controllers are broadly impeded by the discussed absence of accurate and computationally cheap dynamic models. In this design, the summation of the integrated and feedforward terms is a virtual xyz position, the "integrated tip position."

A common alternate framing is to position the IK before the outermost error and place another IK along the feedback path to convert the measured position into estimated joint angles. This joint-space topology has two difficulties in a *redundant* interleaved manipulator: some effort must be taken to ensure that the now-separated IKs seek the same local minima while not compromising their search; and the controller must be prevented from actuating redundant joints in opposing fashions, where the motion is in the task null space. These distinctions are only apparent in nonconvex IK implementations, described as follows.

When executing a trajectory, the desired tip position and the task goal position change every iteration, with the IK continually seeking a new set of joint angles to achieve that task goal. We

[2]As first derived by Camarillo *et al.* [6], a frictionless mechanics model predicts constant curvature; knowing this result, the FK use geometry to convert from tendon displacement to catheter articulation.

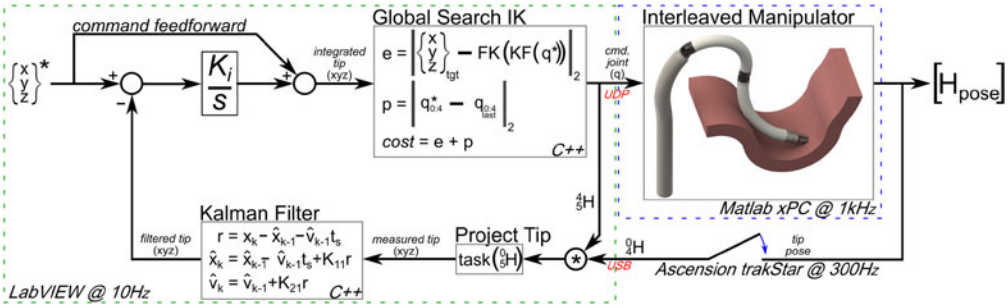

Fig. 3. Multidegree of freedom task space controller. The outer control loop runs at 10 Hz in LabVIEW with the IK and filtering implemented in a C++ library. The servodrives on a MATLAB xPC realtime computer at 1 kHz. The 1-D, 2-state polynomial Kalman filter is used individually on the measured *xyz* tip positions and within the IK on the joint angles, each with unique filter gains.

desire a maximal 3-D (*xyz*) tip position workspace and would like to use the remaining 2-D null-space to reward solutions that minimize joint movement from previous solutions. The IK are implemented in a C/C++ library which calls the NLopt nonlinear optimization library [27, version 2.4.2] and particularly the global, derivative-free, constrained, and objective-scaling DIRECT algorithm of [28]. One satisfactory IK objective, given in Fig. 3, minimizes the sum of the task error norm e and the norm of the difference of the four physical joints from their previous solution p, constrained within the physical joint limits. This objective does not eliminate the manipulator redundancy—the joint movement minimization "task" lies within the tip positioning task—but it does introduce a preference between possible solutions. Even when preferring to minimize the difference between successive solutions in the objective, experiments suffered undesirable chatter due to the solution jumping between multiple solutions. This motivated filtering of the candidate joint solutions within the objective function by a very computationally cheap polynomial Kalman filter [29]. While filtering in the IK search, only the final solution is used in the Kalman state update. As implemented, this filter modifies the objective function to encourage joint position similarity without limiting the global joint angle search. This solution was sufficient for the present effort but will be revisited in the future work.

That future work may also reconsider the applicability of the many varieties of redundant IK methods to a general interleaved manipulator (see [30] for an overview). The application of these methods is typically disappointing due to their assumption that the FK are accurate, which is not generally the case in the continuum manipulators (and particularly here, note the discrepancy in desired and integrated task position in Fig. 5 below). FK error leads to the incremental joint updates not always or even often resulting in the expected gains, which can lead to chatter and impair real-world convergence. (One interesting framing is that of [31] which uses estimates of the actuator joint positions from the measured configuration in the IK. This may improve convergence and solution stability, but accuracy will still be impaired by the FK error.) The performance of the class of Jacobian-inverse solvers is fundamentally limited, as all are typically implemented as simple gradient descent optimizers [30], [32]. Their slow convergence is explained by the general omission of the Wolfe conditions (sufficient decrease and curvature) to compute the necessary step size, while their local nature guarantees they get trapped in local minima [33].

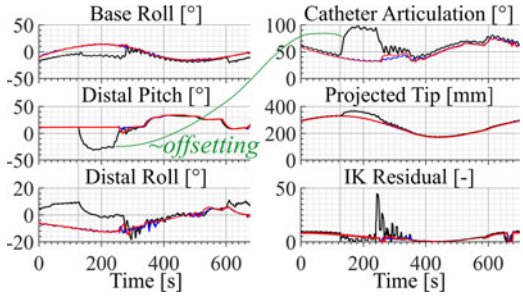

Fig. 4. Joint positions and IK residuals during the circle tracking of Fig. 5. At no point does the IK solver fail to converge; as explained in the text, the large residuals in the 0.09 tuning result from kinematic error while the zero residuals occur when the preceding joint solution is preferred. The red, blue, and black curves have integral controller gains $K_i = 0.06$, 0.07, and 0.09, respectively. The joint limits of $\pm 170°$, $\pm 35°$, $\pm 60°$, 0:280°, and 0:1 m are not encountered.

Alternately, adoption of various task priority methods limits the maximum task dimension to the number of manipulator DOFs and while adding subtasks orthogonal to the primary task can ensure that there is a global minimum, there may not be obvious subtasks to specify the remaining DOFs [32]. In the presence of FK errors and the absence of Jacobian-based methods robust to these errors, the present interleaved manipulator is better served by a more powerful and more general optimization method that avoids these difficulties.

D. Tracking a Virtual Target

In evaluating this interleaved prototype's design and controller, we are chiefly interested in how the controller uses the rigid and flexible joints to minimize error over shifting redundancies. Figs. 4 and 5 track a virtual circle under increasing the controller gain. The experiment begins by converging from the manipulator start position (approximately [910, −280, 91] mm) to the first point in the virtual circle at [1050, 140, −24] mm. Once the position error norm was below approximately 2 mm, the virtual circle target began moving through 7000 points about a 200-mm diameter circle inclined at 30° from horizontal (*YZ*) at 0.1 s/point or 0.9 mm/s. Going this slow avoids excitation of the catheter while helping to clearly show controller-induced errors. No noticeable improvement was observed from independently varying the *x*/*y*/*z* gains on the task error vector in Fig. 3, so $K_i = K_{ix} = K_{iy} = K_{iz} = 0.06$ (red), 0.07 (blue), and 0.09[-]

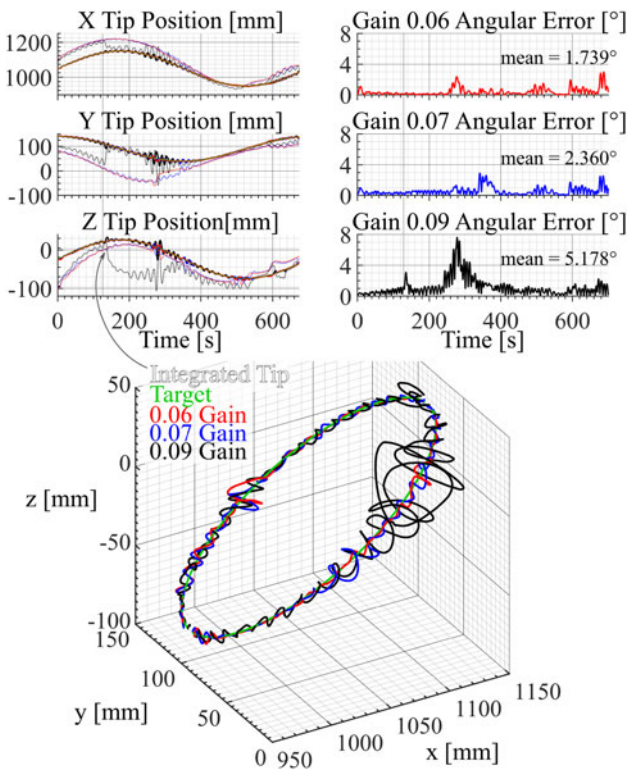

Fig. 5. Tracking a 200-mm-diameter circle under 0.06 (red), 0.07 (blue), and 0.09 (black) integral controller gains. The left column's *x*/*y*/*z* position versus time correspond to a clockwise motion from 12 o'clock about the 3-D circle, with the angular errors given at right. In the left column, dashed lines show the "integrated tip" position noted in Fig. 3, with the green line providing the target position xyz^*. The vertical rule at $t \approx$ 125 s denotes the onset of an IK solution switch (see Fig. 4).

(black) while the joint Kalman filters were adjusted for best performance at each gain. The measurement Kalman filter was tuned to reduce some specific sensor noise apparent across all experiments.

The static geometric parameters of the FK described above were found by commanding simultaneous sinusoids on each of the joints over their joint ranges and fitting the FK-estimated tip position against the measured tip position while varying the parameters. The parameter estimates are close to the measured values; this fitting essentially rebaselines the FK to represent the middle of each joint's actuation range, rather than the initial position. This has the greatest impact on the catheter; rather than basing the FK on the initial straight catheter position, articulating it between 0° and 180° baselines the FK at 90° articulation. The nonlinear effects which we have explicitly omitted from the FK model are thus reduced in our typical actuation range (see Fig. 4) relative to the 0° baseline. (This fitting also reduces the constant bias in the Ascension sensor. The field is known to vary by a few centimeters across its sensing volume. We expect and have observed variations within one centimeter over the dexterous workspace of this prototype—too small and smoothly varying to explain the integrated/commanded discrepancy.) As the FK were implemented in the C/C++ IK library, it was a simple extension to use the same nonlinear optimizer to find the (potentially overfit) FK parameters.

E. Observations

Fig. 4 shows the joint positions and IK residual while tracking the circle of Fig. 5. Notice, first, that increasing the gain led the IK to prefer different base and distal roll orientations than the lesser tunings. The 0.09's larger gain moves the integrated tip (see Fig. 3) across the *xyz* workspace more readily, and in doing so switches between optimal configurations more quickly than the lesser tunings. This switching leads to greater error, as the controller is moving the integrated tip, and hence joint solution faster than the manipulator can move the physical tip. Fig. 5 also shows the measured and integrated *x*, *y*, and *z* tip positions with time. Angular error is defined as the arctangent of the Euclidean error between the target and tip positions and the tip-to-target distance (the fifth, virtual joint position). Using this angular error normalizes the results by distance, which allows comparison between trajectory segments. The 50–100 mm discrepancy between the actual and integrated tip positions evinces substantial errors remaining even after the parameter estimation, though this should be seen as a zeroth-order estimation of a dynamic process. This may be seen in Fig. 5 around $t = 450$ s, where the good agreement between integrated and measured positions indicates that those remaining errors are varying with the configuration; in lieu of more robust manipulator modeling, these parameters should be estimated online.

The vertical rule in Figs. 4 and 5 at $t \approx 125$ s denotes the onset of an IK solution switch in the 0.09 tuning, as it is followed by the large joint movements, momentarily increased task error, and immediately decreased IK residual. While the manipulator executes the large joint motions to achieve the solution switch, the task error continues to integrate; depending on the configuration and the time to realize the new solution, the integrated tip may step across another solution boundary and prefer some different, or the previous, solution. This renders the ongoing motion moot.

As the indicated configuration is not singular, why, then, do the two free DOFs not permit a smooth transition between solutions? Though not singular, there is a substantial redundancy between the catheter and distal pitch actions such that moving orthogonal to the redundancy requires large joint motions (labeled "offsetting" in the figure), and hence large joint velocities between steps that may be limited by the servo's safety rules. The macroresult is that controller stability varies throughout the experiment; it is nearly unstable at some segments and these are what limit the overall integral controller tuning. While the use of a nonlinear gradient-free optimization avoids issues of ill-conditioned matrix inversion near singularities, the velocity limits effectively prevent smooth transitions between minima. This same effect is responsible for the notable increases in error in the 0.06 and 0.07 angular errors at $t = 280$ s (0.06) and $t = 340$ s (0.07), and both at $t = 680$ s. In these cases, the smaller gain moves the integrated tip closer to the speed of the manipulator, allowing the integrated tip movement to be more closely and accurately guided by the real task error. Note that in the experimental data there are no convergence failures (see Fig. 4, lower right); the drops in the IK residual are merely the realization that a better solution is possible with essentially a zero change in the joint angles.

Mechanically, the performance of the 5-D prototype is limited by rigid joint cable stretch, where the flexible shaft windup is minimized by the distal reductions, any stretch in the output cable transmissions is immediately present in the joint actuation. Contributing to the cable stretch is the friction along the cable path, static and dynamic frictions in the joints, and gravity loading of more distal elements. One additional unexpected factor was cable creep, by which the unwoven, multistranded Kevlar cables lengthened through fiber movement. It is hard to gauge the extent of the creep, but close inspection shows several escaped cable fibers—evincing relative fiber movement—and, anecdotally, the rigid joints exhibit greater compliance than when assembled. These effects lead to greater-than-expected output cable compliance which limited the rigid joint performance. With the above limitations, the 5-D manipulator performance is equally limited by the flexible segment hysteresis and rigid joint actuation deadzone, while the safety is notionally improved by the output compliance.

In light of the errors along the controller's forward path, the integral controller performed well. This simple design exploited each of the joints in pursuing the goal across varying redundancies. The task-space IK suffered zero convergence failures over the three tested gains and on most experiments in general; instability arose in the integral controller before the IK diverged. This was clearly encouraged by the free DOF (five joints tracking a 3-D target) and the global search. Some of the discussed obstacles are unique to this design, but many of the general challenges will be encountered by any multiple-degree-of-freedom interleaved manipulator. The circle tracking experiment highlighted the critical importance of accurate FK. Future efforts will tackle these errors directly, but they currently prevent exploration of possible performance gains. The next experiment investigates the performance gain directly through a simplified system.

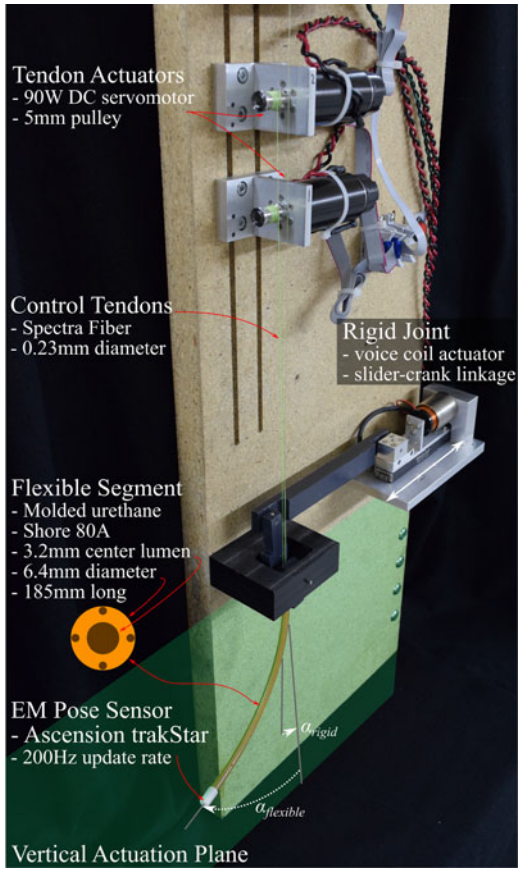

Fig. 6. Single-DOF performance testbed. The 185-mm-long catheter segment is actuated in a vertical plane by two dc motors. The rigid joint moves in the same vertical plane via a slider-crank mechanism actuated by a voice coil. Manipulator articulation is measured by the same electromagnetic pose sensor as before.

IV. Simplified Performance Testbed

The complexity of the 5-D clinically approximate prototype manipulator prevented basic explorations into whether interleaved manipulation can increase task performance. A simple single-DOF system illumines some of the fundamental performance characteristics that might be encountered in a clinical interleaved manipulator. Recalling our desire to decouple safety and actuation, this system substantially entrusts safety to the flexible catheter segment and performance to the rigid joint. Considering only a single-DOF greatly simplified the design, construction, analysis, and interpretation, leading to a quick validation of the potential of interleaved manipulation.

We presented initial results of this single-DOF testbed in [34], but that experiment was sensor-limited to small motions near zero articulation. After describing the testbed and redundant controllers, we present results at articulations of 11° and 220°, with an unexpected observation of the effect of rigid joint saturation.

A. Overview of the Single-DOF Testbed

The single DOF manipulator in Fig. 6 consists of a single articulating flexible segment and a proximal revolute joint arranged redundantly. The flexible segment is a molded 6.4 mm diameter by 185-mm urethane body with four tendon guide lumens and a central 3.2-mm instrument lumen. This catheter is articulated using a pair of opposing control tendons (Honeywell Spectra fiber, 0.23 mm diameter) anchored at the tip and pulled by a pair of 90-W dc motors (#273754 Maxon Motor AG) with 5-mm diameter pulleys. The tendon position controller (operating on the motor encoder) has a closed-loop bandwidth of approximately 35 Hz. Actuation of the tendons causes the flexible segment to articulate within a vertical plane.

The rigid joint motion provides rotation about a pivot axis located at the base of the flexible segment which is perpendicular to the flexible segment actuation plane. The flexible segment control tendons intersect the rotation axis of the rigid joint to eliminate coupling between the flexible and rigid motions. The rigid joint rotation is accomplished through a slider-crank mechanism actuated by a voice-coil motor (BEI Kimco Magnetics) with approximately 6 mm of travel which results in approximately $\pm 16°$ of manipulator articulation (when the flexible segment is unarticulated). Catheter tip motion is acquired with the same Ascension trakSTAR electromagnetic pose sensor, providing a globally referenced measurement of the catheter's tip pose at approximately 200 Hz. The controller is implemented

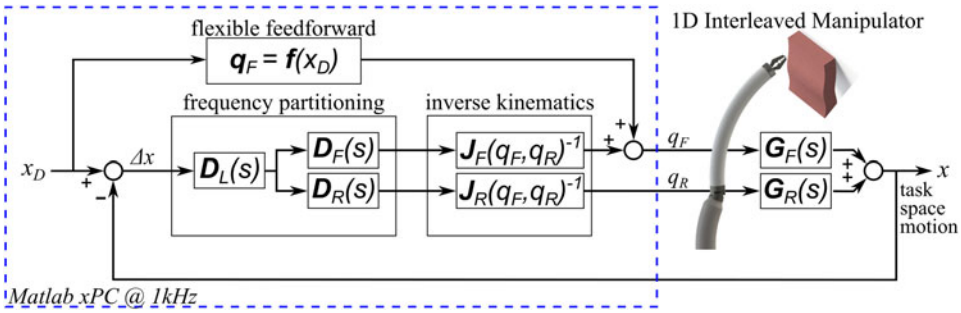

Fig. 7. Overview of a frequency-partitioning single-input multiple-output controller based on [35].

using MATLAB xPC 2009a (Mathworks, USA) on a 3.0-GHz Intel Pentium 4 computer.

B. Single-Input Multiple-Output Controller

One of the central challenges of the interleaved approach is formulating an effective control strategy. There have been many formal methods developed for multiple-input-multiple-output control system design including μ-synthesis, H_∞, and, more recently, design approaches developed for dual-input-single-output systems like the PQ approach of Schroeck *et al.* [35] used here (see [35] for a detailed theoretical description). In this testbed, we pair a typical tendon-actuated flexible segment with a high-precision and -speed, limited range rigid joint, as depicted in Fig. 6. The differences between the flexible and rigid joints suggest a parallel control structure which explicitly partitions the task error signal Δx into high- and low-frequency components. In the context of the overall control structure given in Fig. 7, the flexible segment and rigid-link task-space controllers ($D_f(s)$ and $D_r(s)$) perform this partitioning function while helping to shape the actuator closed-loop dynamics. In addition, a task-space loop compensation block $D_l(s)$ is included to compensate the additional dynamics that result from the parallel path summation of the rigid and flexible segment control signals. The high/low-frequency partitioning is motivated by the desire to limit the motion of the limited-stroke rigid joints while correcting for motion errors that result from the slower responding flexible segments.

The flexible segment control includes a feedforward IK block which converts the desired task space configuration to flexible segment joint commands (segment curvatures). As shown in Fig. 7, the task space control signal is transformed to joint space motion commands via the flexible segment and rigid joint Jacobians J_f and J_r, respectively, under the assumption that the task space error is small. While the rigid joint position will likely closely track the desired motion, the flexible segment is expected to have a significant error and, thus, direct measurement of its motion is required to properly form the Jacobian for both the flexible segment and rigid joints.

While the specific structure of the compensation blocks—$D_f(s)$, $D_r(s)$, and $D_l(s)$ in Fig. 7—vary depending on the system dynamics and the performance goals, there are general considerations for both the flexible segment and rigid joint control that influence the compensator design. In general, robotic catheter systems control tendon actuator position, rather than, say, tendon tension. The low torque density of electromagnetic actuators (used almost exclusively in the type of cardiac interventional catheters under consideration here) generally requires the use of a gear reducer. The resulting increase in a reflected inertia and friction amplification makes tension control difficult to be implemented in a robust manner. As such, the local joint controllers (tendon and rigid joint) have significantly faster closed-loop dynamics than those of the overall closed-loop interleaved manipulator.

To compensate for steady-state flexible segment motion errors, integral control (and variants thereof such as lag compensation) has been successfully applied in the reduction of catheter kinematic errors, e.g., [36]. In the single-DOF interleaved controller, it is the flexible segment compensation block $D_f(s)$ that takes on an integral structure K_i/s. As described in [35], the ratio of joint control compensators ($D_{f/r}(s) = D_f(s)/D_r(s)$) can be used to examine the frequency partitioning characteristics of the compensator design. Assuming that the magnitude of $D_{f/r}(s)$ decreases with increasing frequency, the crossover frequency $\omega_{f/r}$ of $D_{f/r}(s)$ is the point where the magnitudes of $D_f(s)$ and $D_r(s)$ are equal and, thus, the frequency at which the low- and high-frequency partitioning of the control input occurs. Here, the integral gain of $D_f(s)$ was adjusted to maintain stability, arriving at $\omega_{f/r} = 0.05$ Hz; below this the flexible segment primarily acts on the task error and above this the rigid link. With $D_f(s) = K_i/s$, a suitable choice for the rigid joint controller is unity gain $D_r(s) = 1$.

Assuming that the rigid-link and flexible segment system plant transfer functions have constant gain and no phase distortion at low frequencies (i.e., $G_f(s) = G_r(s) = 1$), a reasonable choice for $D_l(s)$ is a simple integral compensator. The gain was adjusted until signs of instability were observed, resulting in a system open-loop crossover frequency of approximately 0.6 Hz. This crossover frequency is chosen to be above the $D_{f/r}(s)$ partitioning frequency, to be below the catheter's first mode of $\sim$1.8 Hz, and to maintain sufficient stability margins.

C. Single-DOF Performance

To evaluate the performance, the interleaved system and one consisting of only the flexible segment were compared. The flexible segment only system was formed by preventing rigid joint motion while using the same flexible segment as the

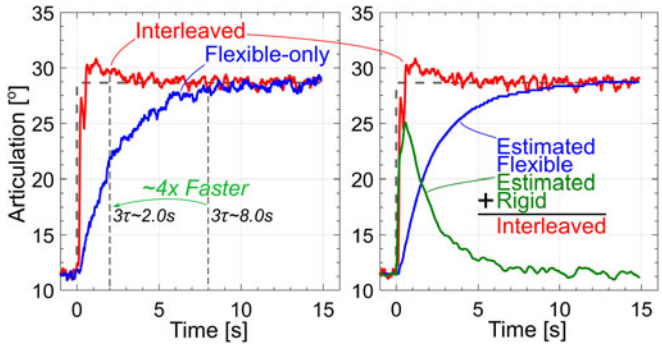

Fig. 8. Experimental response of the interleaved testbed to a commanded step of 17° from an initial articulation of 11.5°. Left: Response of interleaved system (red) and response of flexible segment only manipulator (blue); Right: Total response of the interleaved system (red, same as on the left), estimated flexible segment contribution (blue), and estimated rigid-link contribution (green).

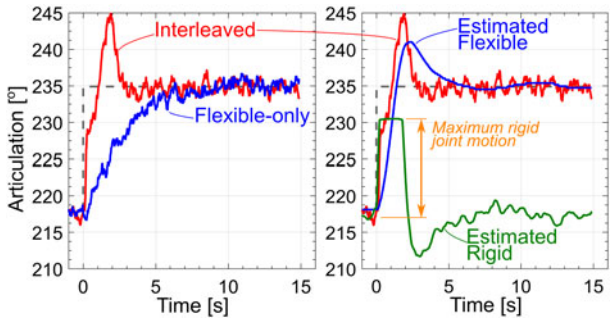

Fig. 9. Experimental response of the interleaved testbed starting from a large initial end-point articulation. Response of the system to a commanded step of 17° from an initial articulation of 218°. Left: Response of interleaved system (red) and response of flexible segment only manipulator (blue). Right: Response of interleaved system (red), estimated flexible segment contribution (blue), and estimated rigid-link contribution (green). The prominent overshoot is due to plant dynamics that change with configuration: applying the same tendon displacement increment in low- and highly articulated configurations gives greater incremental articulation from higher initial articulation. Increasing articulation also decreases the rigid joint-to-tip distance, decreasing the rigid joint's influence. These opposed characteristics lead to greater flexible segment articulation, and less rigid joint articulation, than in the low articulation of Fig. 8 with the resulting rigid joint saturation and tip overshoot.

interleaved system. To provide a clear comparison of the control behavior of each system, the flexible segment feedforward term in Fig. 7 was set equal to zero in both the interleaved and flexible segment only implementations.

The performance of the two systems was evaluated with a simple step response, with the task defined by the catheter tip articulation noted as α in Fig. 6. In the first experiment, the manipulator was positioned approximately in the center of its workspace (vertical) and biased slightly positively ($\sim 11^\circ$) to eliminate any effects of control tendon slack. A small articulation step command ($\sim 17^\circ$) was applied and the position control performance was measured. Fig. 8 shows the results of this first low articulation experiment. The left pane of Fig. 8 demonstrates that the response of the interleaved system is approximately four times faster than the flexible segment only closed-loop system—primarily due to the ability of the rigid joint to effect changes in articulation faster than the more compliant flexible segment control tendons allow.

To gain a better understanding of the interleaved response, the right pane of Fig. 8 shows a projection of the actuator encoder data into the task space to estimate the contribution of each actuator to the total tip articulation. Note that this projection does not include catheter dynamics and therefore has some inherent error. Nevertheless, Fig. 8 clearly shows the effect of the frequency partitioning between the slower flexible segment and faster rigid joint controllers. The response of the rigid joint actuator is almost immediate, reacting to the high-frequency content contained in the step input command. As the slower flexible segment actuator motion increases, the rigid link joint actuator motion decreases in magnitude, returning it to the center of its actuation range. The summation of the two results in a faster response as compared to the flexible segment alone.

In a second experiment, the same step command was applied (17°) with the manipulator initially positioned with an articulation of 218° (a U-shaped initial configuration). As seen in Fig. 9, left, the response of the interleaved system suffers from a substantial overshoot primarily due to the saturation of the rigid joint. As before, Fig. 9, right, projects the actuator encoder data into the task space to estimate the contribution of each actuator to the total tip articulation. The obvious saturation of the rigid link joint leads the flexible segment to overshoot the command with a corresponding effect on the overall system response.

To understand the source of the response overshoot and explore the effects of rigid joint saturation on the overall system stability, a series of similar step response experiments were carried out where limitations on the rigid joint range of motion were emulated by restricting commands to the rigid-link position controller, as in Fig. 10. As the rigid joint range of motion is reduced the response becomes more oscillatory. In the extreme case, where the rigid joint motion is set equal to zero, the system becomes unstable.

The reduction in system stability can be seen in the system's stability margins as a function of joint saturation levels. To capture this, we constructed a model of the compensated open-loop system which is consistent with experimental frequency response measurements and examine in Fig. 10 the effects of the rigid joint saturation via a gain along the rigid joint path (a continuous approximation to a nonlinear saturation function, as in [37]). The overall system closed-loop stability can be determined as a function of rigid joint saturation by evaluating the phase and gain margin of the compensated open-loop system as the saturation gain K_s is varied from 1.0 (no saturation) to 0.0 (total saturation).

As shown in Fig. 10, the nominal compensated open-loop interleaved system (with no saturation) has closed-loop phase and gain margins of approximately 80° and 0.6 dB, respectively. The nominal system stability margins reflect the design objective where by the highest possible closed-loop bandwidth was sought. Here, the closed-loop bandwidth is restricted by the first vibrational mode of the flexible segment. The lightly damped mode is responsible for the low gain margin while the integral

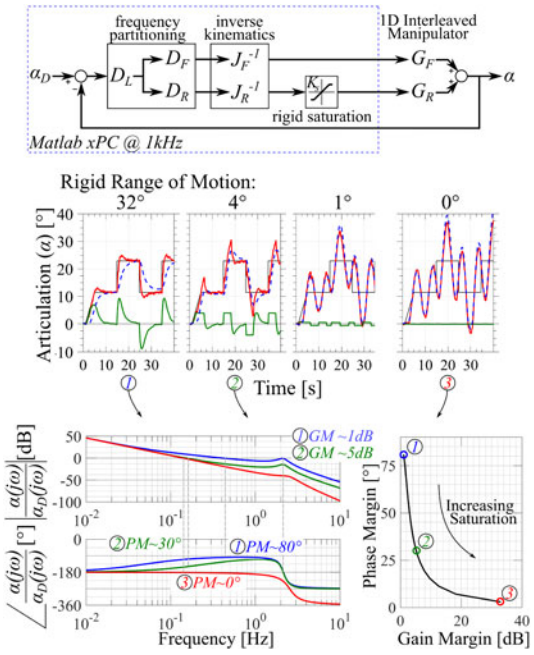

Fig. 10. Top: Rigid link saturation is approximated with a variable gain K_s as described by [37]. Middle: Step response under increasing saturation. From left: Full rigid joint range of motion demonstrates performance similar to that in Fig. 8; decreasing to 4° shows lengthier convergence and large overshoot, reminiscent of Fig. 9; 1° is marginally stable; and 0° of actuation range is unstable. Bottom: Interleaved system stability margins as a function of joint saturation levels. The degradation of the overall system stability (as evidenced by the reduction in phase margin) is shown in the Bode plot (left) and the phase-versus-gain plot.

control action results in a robust phase margin in excess of 80°. As the rigid link joint saturation increases (approximated by a reduction in K_s), the resulting system phase margin decreases, resulting in a closed-loop response which is lightly damped. At the extreme, where the saturation is total (no rigid joint motion), the system's phase margin approaches zero, resulting in a highly oscillatory response. In practice, unmodeled system dynamics would lead to an unstable system. As such, the effects of saturation should be carefully considered in the design of any interleaved system.

D. Single-DOF Observations

This single-DOF testbed and frequency-partitioned controller demonstrate fundamental properties of an interleaved manipulator: joint characteristics (accuracy, range, and speed) can be combined into a single manipulator and overall system performance may be increased through a controller aware of those characteristics. The described controller demonstrates one potential method of realizing faster response speed and greater accuracy in an interleaved manipulator. The variable redundancies present in higher dimensions limit its direct application to practical manipulators, but the performance improvements demonstrate the benefits of a frequency-partitioning approach. The three-times performance improvement of Fig. 8 is slightly better than that of [22], but note that, conceptually, an interleaved manipulator's modal controller could use the rigid joints for the modal decoupling, decreasing the tendon-coupled disturbances on the continuum segments and increasing the manipulator performance over the continuum-only manipulator. That said, the gains attainable by a noncollocated closed-loop controller are fundamentally limited by the flexible segment's first vibrational mode, though we believe that further improvements are possible.

V. Looking Forward

The fundamental limitation of the single-DOF testbed was the catheter's first vibrational mode, while the 5-D prototype suffered most significantly from large and variable kinematic errors. These large errors made tuning the 5-D controller difficult and resulted in a rather anemic performance. We expect an improved performance from a deeper consideration of the kinematic errors and the development of a dynamic parameter estimator. The aim is to improve the open-loop characteristics so that the closed-loop controller sees less error; this will also encourage similarity between the controller and physical IK solution spaces. The control design and tuning of the 5-D prototype were complicated by coupling between the joints and flexible segment hysteresis. Partitioning the task error by frequency, as in Section IV, is an attractive, intuitive use of the joint redundancy; additional development may realize some form of this concept in the 5-D manipulator as part of an exploration of various IK objectives.

To conclude, we revisit the interleaved continuum-rigid concept in Fig. 1. In both experimental systems, the flexible catheter segments are essential for safely accessing a large workspace. Diligent mechanism and control design allows actuation nonlinearities to be compensated by the limited-extent rigid joints. The added redundancy increases task dexterity and performance, and may allow the complete avoidance of flexible segment actuation nonlinearities. These benefits open a here-to-fore unappreciated avenue for increasing the continuum manipulator's capability in challenging environments.

References

[1] J. Burgner-Kahrs, D. C. Rucker, and H. Choset, "Continuum robots for medical applications: A survey," *IEEE Trans. Robot.*, vol. 31, no. 6, pp. 1261–1280, Dec. 2015.

[2] Z. Issa, J. M. Miller, and D. P. Zipes, *Clinical Arrhythmology and Electrophysiology: A Companion to Braunwald's Heart Disease.* Amsterdam, The Netherlands: Elsevier, 2012, ch. 15.

[3] J. G. Andrade, L. Rivard, and L. Macle, "The past, the present, and the future of cardiac arrhythmia ablation," *Can. J. Cardiol.*, vol. 30, no. 12, pp. s431–s441, Dec. 2014.

[4] M. Wright and S. M. Narayan, "Ablation of atrial fibrillation," *Trends Cardiovascular Med.*, vol. 25, no. 5, pp. 409–419, Jul. 2015.

[5] D. Trivedi, C. D. Rahn, W. M. Kier, and I. D. Walker, "Soft robotics: Biological inspiration, state of the art, and future research," *Appl. Bionics Biomechanics*, vol. 5, no. 3, pp. 99–117, 2008.

[6] D. B. Camarillo, C. F. Milne, C. R. Carlson, M. R. Zinn, and J. K. Salisbury, "Mechanics modeling of tendon-driven continuum manipulators," *IEEE Trans. Robot.*, vol. 24, no. 6, pp. 1262–1273, Dec. 2008.

[7] D. B. Camarillo, C. R. Carlson, and J. K. Salisbury, *Task-Space Control of Continuum Manipulators With Coupled Tendon Drive*, (Springer Tracts in Advanced Robotics Series). New York, NY, USA: Springer, 2009, vol. 54, ch. Experimental Robotics, pp. 271–280.

[8] R. J. Webster III and B. A. Jones, "Design and kinematic modeling of constant curvature continuum robots: A review," *Int. J. Robot. Res.*, vol. 29, no. 13, pp. 1661–1683, 2010.

[9] G. Subramani and M. R. Zinn, "Tackling friction-an analytical modeling approach to understanding friction in single tendon driven continuum manipulators," in *Proc. 2015 IEEE Int. Conf. Robot. Autom.*, May 2015, pp. 610–617.
[10] J. Jung, R. S. Penning, and M. R. Zinn, "A modeling approach for robotic catheters: Effects of nonlinear internal device friction," *Adv. Robot.*, vol. 28, no. 8, pp. 557–572, 2014.
[11] M. Khoshnam and R. V. Patel, "Robotics-assisted catheter manipulation for improving cardiac ablation efficiency," in *Proc. 2014 5th IEEE RAS EMBS Int. Conf. Biomed. Robot. Autom. Soc. Eng. Med. & Biol. Soc.*, 2014, pp. 308–313.
[12] S. Kesner and R. Howe, "Position control of motion compensation cardiac catheters," *IEEE Trans. Robot.*, vol. 27, no. 6, pp. 1045–1055, Dec. 2011.
[13] A. Melingui, R. Merzouki, J. Mbede, C. Escande, and N. Benoudjit, "Neural networks based approach for inverse kinematic modeling of a compact bionic handling assistant trunk," in *Proc. 2014 IEEE 23rd Int. Symp. Ind. Electron.*, 2014, pp. 1239–1244.
[14] M. Rolf and J. Steil, "Efficient exploratory learning of inverse kinematics on a bionic elephant trunk," *IEEE Trans. Neural Netw. Learn. Syst.*, vol. 25, no. 6, pp. 1147–1160, Jun. 2014.
[15] M. Giorelli, F. Renda, M. Calisti, A. Arienti, G. Ferri, and C. Laschi, "Neural network and Jacobian method for solving the inverse statics of a cable-driven soft arm with nonconstant curvature," *IEEE Trans. Robot.*, vol. 31, no. 4, pp. 823–834, Aug. 2015.
[16] G. Bian, M. Lipowicz, and G. H. Kruger, "Self-learning of inverse kinematics for feedforward control of intracardiac robotic ablation catheters," in *Proc. Pattern Recog. Assoc. South Africa Robot. Mechatronics Int. Conf.*, 2015, pp. 72–77.
[17] D. Bristow, M. Tharayil, and A. Alleyne, "A survey of iterative learning control," *IEEE Control Syst.*, vol. 26, no. 3, pp. 96–114, Jun. 2006.
[18] M. Ivanescu, D. Popescu, and N. Popescu, "A decoupled sliding mode control for a continuum arm," *Adv. Robot.*, vol. 29, no. 13, pp. 831–845, 2015.
[19] V. Falkenhahn, A. Hildebrandt, R. Neumann, and O. Sawodny, "Model-based feedforward position control of constant curvature continuum robots using feedback linearization," in *Proc. 2015 IEEE Int. Conf. Robot. Autom.*, 2015, pp. 762–767.
[20] R. H. Cannon and E. Schmitz, "Initial experiments on the end-point control of a flexible one-link robot," *Int. J. Robot. Res.*, vol. 3, no. 3, pp. 62–75, 1984.
[21] A. Preumont, *Vibration Control of Active Structures: An Introduction* (Solid Mechanics and its Applications Series), vol. 96, G. M. L. Gladwell, Ed., 2nd ed. Norwell, MA, USA: Kluwer, 2002.
[22] R. Penning and M. Zinn, "A combined modal-joint space control approach for minimally invasive surgical continuum manipulators," *Adv. Robot.*, vol. 28, no. 16, pp. 1091–1108, 2014.
[23] L. S. Cowan and I. D. Walker, "The importance of continuous and discrete elements in continuum robots," *Int. J. Adv. Robot. Syst.*, vol. 10, pp. 1–13, 2013.
[24] B. Conrad and M. Zinn, "Closed loop task space control of an interleaved continuum-rigid manipulator," in *Proc. 2015 IEEE Int. Conf. Robot. Autom.*, 2015, pp. 1743–1750.
[25] B. L. Conrad and M. R. Zinn, "Interleaved continuum-rigid manipulation approach: Development and functional evaluation of a clinical scale manipulator," in *Proc. 2014 IEEE/RSJ Int. Conf. Intell. Robot. Syst.* Sep. 2014, pp. 4290–4296.
[26] D. B. Camarillo, C. R. Carlson, and J. K. Salisbury, "Configuration tracking for continuum manipulators with coupled tendon drive," *IEEE Trans. Robot.*, vol. 25, no. 4, pp. 798–808, 2009.
[27] S. G. Johnson. (2015). The NLopt nonlinear-optimization package. [Online]. Available: http://ab-initio.mit.edu/nlopt
[28] D. R. Jones, C. D. Perttunen, and B. E. Stuckman, "Lipschitzian optimization without the Lipschitz constant," *J. Optimiz. Theory Appl.*, vol. 79, no. 1, pp. 157–181, 1993.
[29] P. Zarchan and H. Musoff, *Fundamentals of Kalman Filtering: A Practical Approach*, (ser. Progress in Astronautics and Aeronautics), P. Zarchan, Ed. Washington, DC, USA: Amer. Inst. Aeronaut. Astronaut., 2005, vol. 208.
[30] A. Colome and C. Torras, "Closed-loop inverse kinematics for redundant robots: Comparative assessment and two enhancements," *IEEE/ASME Trans. Mechatronics*, vol. 20, no. 2, pp. 944–955, Apr. 2015.
[31] B. Bardou, P. Zanne, F. Nageotte, and M. de Mathelin, "Control of a multiple sections flexible endoscopic system," in *Proc. 2010 IEEE/RSJ Int. Conf. Intell. Robot. Syst.*, 2010, pp. 2345–2350.
[32] S. Chiaverini, G. Oriolo, and I. D. Walker, *Springer Handbook of Robotics*. New York, NY, USA: Springer, 2008, ch. 11.
[33] J. Nocedal and S. Wright, *Numerical Optimization*. New York, NY, USA: Springer, 2006.
[34] B. L. Conrad, J. Jung, R. S. Penning, and M. R. Zinn, "Interleaved continuum-rigid manipulation: An augmented approach for robotic minimally-invasive flexible catheter-based procedures," in *Proc. 2013 IEEE Int. Conf. Robot. Autom.*, 2013, pp. 718–724.
[35] S. J. Schroeck, W. C. Messner, and R. J. McNab, "On compensator design for linear time-invariant dual-input single-output systems," *IEEE/ASME Trans. Mechatronics*, vol. 6, no. 1, pp. 50–57, Mar. 2001.
[36] R. S. Penning *et al.*, "Towards closed loop control of a continuum robotic manipulator for medical applications," in *Proc. 2011 IEEE Int. Conf. Robot. Autom.*, 2011, pp. 4822–4827.
[37] K. Ogata, *System Dynamics*, 3rd ed. Englewood Cliffs, NJ, USA: Prentice-Hall, 1998.

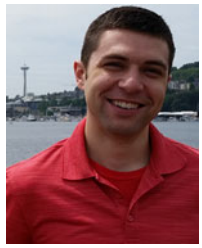

Benjamin L. Conrad (S'12) received the B.S. degree in engineering mechanics-astronautics and the M.S. degree in mechanical engineering from the University of Wisconsin, Madison, WI, USA, in 2010 and 2013, respectively.

His research interests include mechanical and control design of electro-mechanical systems for use in challenging environments.

Michael R. Zinn (M'07) received the B.S. and M.S. degrees from Massachusetts Institute of Technology, Cambridge, MA, USA, in 1987 and 1988, respectively, and the Ph.D. degree in mechanical engineering from Stanford University, Stanford, CA, USA, in 2005.

He joined the faculty at the University of Wisconsin, Madison, WI, USA, in 2007. Prior to joining the University of Wisconsin, Madison faculty, he was the Director of Systems and Controls Engineering at Hansen Medical where he helped to develop the world's first commercially available minimally invasive flexible surgical robotic system. In addition to his experience at Hansen Medical, he has more than ten years of electro-mechanical system design and manufacturing experience in aerospace and high-technology industries. His research interests include understanding and overcoming the design and control challenges of complex electro-mechanical systems with a primary focus on human-centered robotics. His focus on human-centered robotics spans multiple application areas including manufacturing, medical devices, and haptics.